Suplemento de la Revista Mexicana de Física **3** 0308029 (2022) 1–6

The two-step mechanism explaining the dibaryon "$d^*(2380)$" peak

R. Molina and E. Oset

Departamento de Física Teórica and IFIC, Centro Mixto Universidad de Valencia-CSIC, Institutos de Investigación de Paterna, Apartado 22085, 46071 Valencia, Spain

N. Ikeno

Department of Agricultural, Life and Environmental Sciences, Tottori University, Tottori 680-8551, Japan.

Received 14 January 2022; accepted 2 March 2022

In this talk we show that the two-step sequential one pion production mechanism, $np(I=0) \to \pi^- pp$, followed by the fusion reaction $pp \to \pi^+ d$, can explain the narrow peak identified with a "$d^*(2380)$" dibaryon in the $np \to \pi^+\pi^- d$ reaction with $\pi^+\pi^-$ in $I=0$. We demonstrate that the second step $pp \to \pi^+ d$ is driven by a triangle singularity that determines the position of the peak of the reaction and the large strength of the cross section. The combined cross section of these two mechanisms produce a narrow peak with the position, width and strength compatible with the experimental observation within the approximations done. This novel interpretation of the peak without invoking a dibaryon explains why the peak is not observed in other reactions where it has been searched for.

Keywords: Dibaryon; hexaquark; two-nucleon fusion.

DOI: https://doi.org/10.31349/SuplRevMexFis.3.0308029

1. Introduction

The $np \to \pi^0\pi^0 d$ reaction exhibits a sharp peak around 2370 MeV with a narrow width of about 70 MeV, and is also seen in the $pp \to \pi^+\pi^- d$ reaction with approximately double strength [1–3], which has been identified with a dibaryon peak, namely, the $d^*(2380)$. Interestingly, in an old work written by Bar-Nir *et al.* [4] a peak with poor statistics, already visible for the $np \to \pi^+\pi^- d$ reaction was explained from a different mechanism: two-step sequential π production, $np \to pp\pi^-$ followed by $pp \to \pi^+ d$. The cross section for $np \to \pi^+\pi^- d$ was evaluated factorizing cross sections for the two latter reactions in an "on-shell" approach that called for further checks concerning its accuracy. Such mechanism has no further been invoked concerning the new improved data on the $np \to \pi^+\pi^- d$, $np \to \pi^0\pi^0 d$ reactions [1–3]. Following this idea, the mechanism for $np \to \pi^+\pi^- d$ can be expressed diagrammatically as in Fig. 1.

For the first step, $np \to \pi^- pp$, we have now much more refined data [5, 6]. In [5] a Lorentzian fit with a mass of $m = 2315$ MeV and $\Gamma = 150$ MeV corresponding to the intermediate state $N^*(1440)N$ was done to the data. The process with a t-channel Roper excitation was investigated earlier in Ref. [7], however no peak is obtained in the same energy region.

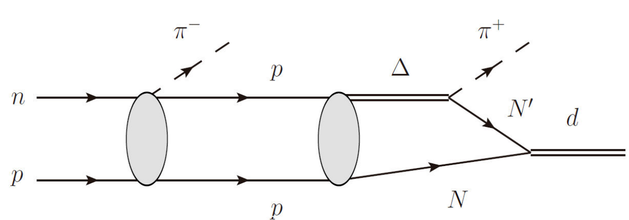

FIGURE 1. Two step mechanism for $np \to \pi^+\pi^- d$ suggested in [4] with explicit Δ excitation in the $pp \to \pi^+ d$ last step as found in Ref. [8–10]. The mechanism with the nn intermediate state is considered in addition.

In the second step, the time reversal reaction of $pp \to \pi^+ d$, π^+ absorption in the deuteron, $\pi^+ d \to pp$ has been investigated in Ref. [8–10], concluding that it is dominated by a Δ excitation. Data on this reaction and its time reversal are available in Ref. [11].

In view of the more precise data on the $np \to \pi^+\pi^- d$, $np \to \pi^0\pi^0 d$ [1–3, 12], and $np(\mathrm{I}=0) \to \pi^- pp$ [5, 6] cross sections, and the recent developments [13] on triangle singularities [14, 15] it is worth to come back to this issue. First, we show that the $pp \to \pi^+ d$ reaction is driven by a triangle singularity. Then, we test whether the two-step mechanism [4] of Fig. 1 can explain the dibaryon peak.

2. Triangle singularity in the $pp \to \pi^+ d$ reaction

Triangle singularities (TS) were introduced in the 60's by R. Karplus and L. D. Landau in Refs. [14, 15]. They stem from a Feynman diagram with a loop with three intermediate particles which develops a singularity when the three intermediate particles can be placed simultaneously on shell and they are collinear in a way as to satisfy the Coleman-Norton theorem [16]. The Coleman-Norton theorem expressed for the present case, see Fig. 2, can be understood in the following way: the pp system produces a Δ and a nucleon N, back to back in the pp rest frame. The Δ decays into $\pi N'$, with the π in the direction of the Δ and N' in its opposite direction, which is then the direction of N. The N' goes faster than N (implicit in Eq. (18) of Ref. [13]) and after a while catches up

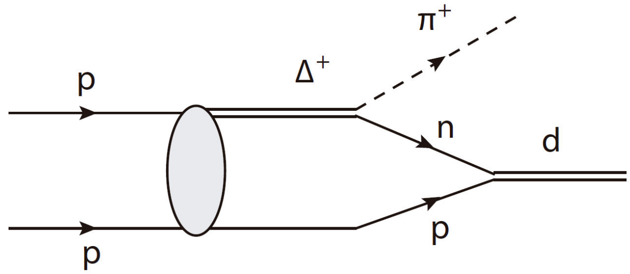

FIGURE 2. Mechanism for pion production with Δ excitation and np fusion in the deuteron.

with N and they fuse to give the deuteron. This natural possibility, inherent to a TS, makes the cross section large, unlike other fusion reactions which rely upon large momentum components of the deuteron wave function, or equivalently, very far off shell nucleons in the intermediate states of the loop.

The two different topologies present in this reaction are depicted in Fig. 3. We take an antisymmetrized pp system with

$$|pp\rangle \equiv \frac{1}{\sqrt{2}}\left(|\vec{p}, s_1; -\vec{p}, s_2\rangle - |-\vec{p}, s_2; \vec{p}, s_1\rangle\right), \quad (1)$$

being $\vec{p}$ the momentum of one proton in the pp rest frame and s_1, s_2 their spin third components. The isospin wave function of the deuteron is $|d\rangle \equiv (1/\sqrt{2})|pn - np\rangle\, \chi_d$, with χ_d any of the three spin 1 states ($\uparrow\uparrow$, $(1/\sqrt{2})(\uparrow\downarrow + \downarrow\uparrow)$, $\downarrow\downarrow$). The vertices involved in these diagrams are πNN, $\pi N\Delta$ and npd vertices. The first one is given by,

$$-i\delta H_{\pi NN} = \frac{f}{m_\pi}\vec{\sigma}\cdot\vec{q}\,\tau^\lambda; \qquad f = 1.00, \quad (2)$$

for a π entering the N line with momentum $\vec{q}$, with $\vec{\sigma}$, $\vec{\tau}$ the spin, isospin Pauli matrices, respectively, and λ the pion isospin in spherical basis. The second one is

$$-i\delta H_{\pi N\Delta} = \frac{f^*}{m_\pi}\vec{S}^\dagger\cdot\vec{q}\,T^{\dagger\lambda}; \qquad f^* = 2.13, \quad (3)$$

with $\vec{S}^\dagger$, $T^{\dagger\lambda}$ the spin, isospin transition operator from spin, isospin $1/2$ to $3/2$, respectively.

In field theory, the deuteron appears in a vertex of type $g_d\theta(q_{\rm max} - |\vec{p}_d^{\,\rm CM}|)$ where $\vec{p}_d^{\,\rm CM}$ is the nucleon momentum of the deuteron in the d rest frame, but it is also possible to use a realistic deuteron wave function [17]. We also used the deuteron wave function of [18] and concluded that the results barely change. We find that

$$-it^\pi_{ij} = -g_d\frac{4\sqrt{2}}{3}\left(\frac{f^*}{m_\pi}\right)^2\left(\frac{f}{m_\pi}\right)\int\frac{d^3q}{(2\pi)^3}\mathcal{F}_\pi(\vec{q})$$
$$\times\left\{Q^{\rm (up)}_{ij}F(\vec{p},\vec{q},\vec{p}_\pi) - Q^{\rm (down)}_{ij}F(-\vec{p},\vec{q},\vec{p}_\pi)\right\}. \quad (4)$$

The function $F(\vec{p},\vec{q},\vec{p}_\pi)$ is given in Appendix B of [17], and the matrix elements of the spin operators are calculated in Appendix C of [17], as $Q^{\rm up}_{ij}$, $Q^{\rm down}_{ij}$ for $i = \uparrow\uparrow, \uparrow\downarrow$, and $j = \uparrow\uparrow$, $(1/\sqrt{2})(\uparrow\downarrow + \downarrow\uparrow)$, $\downarrow\downarrow$. One also needs to multiply by two the

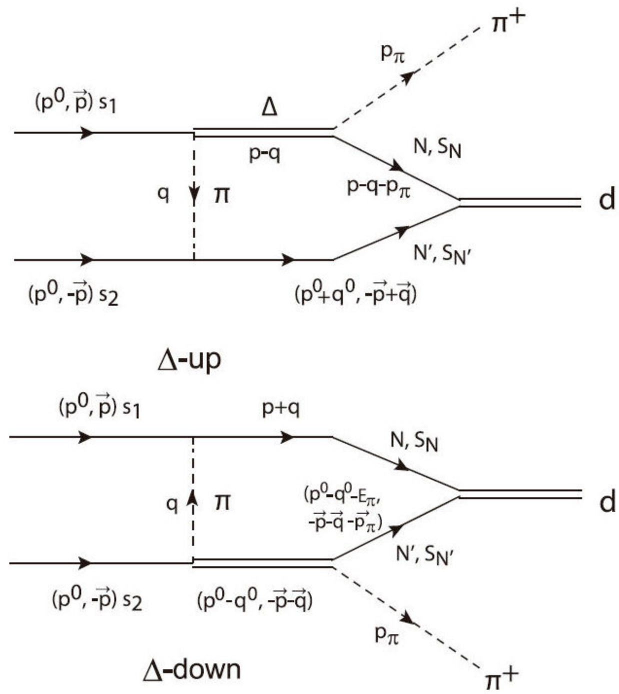

FIGURE 3. The two topological structures, Δ-up and Δ-down contributing to the $pp \to \pi^+ d$ reaction.

sum and average over spins of $|t^\pi|^2$ to account for the initial states $\downarrow\downarrow$, $\downarrow\uparrow$ contributions. Thus,

$$\overline{\sum}\sum|t^\pi|^2 = 2\frac{1}{4}\sum_{i,j}|t^\pi_{ij}|^2 = \frac{1}{2}\sum_{i,j}|t^\pi_{ij}|^2. \quad (5)$$

The cross section for $pp \to \pi^+ d$ is then given by

$$\frac{d\sigma}{d\cos\theta_\pi} = \frac{1}{4\pi}\frac{1}{s}(M_N)^2\, M_d\,\frac{p_\pi}{p}\,\overline{\sum}\sum|t^\pi|^2, \quad (6)$$

where $\cos\theta_\pi$ is $\vec{p}\cdot\vec{p}_\pi/|\vec{p}||\vec{p}_\pi|$. Note that the cuts responsible for the TS appear implicitly in the $F(\vec{p},\vec{q},\vec{p}_\pi)$ function [13, 17]. Other contributions as ρ-exchange, short range correlations between NN and $N\Delta$, and the impulse approximation are also considered. See [17] for more details. Altogether the final cross section is given by Eq. (6) substituting $|t^\pi|$ by $|t|^2$. Thus, in Eq. (5) we make the replacement

$$\sum_{ij}|t_{ij}|^2 \longrightarrow \sum_{ij}|t^\pi_{ij} + t^\rho_{ij} + t^{\rm corr.}_{ij} + t^I_{ij}|^2\,. \quad (7)$$

We thus sum t^π, t^ρ, $t^{\rm corr.}$, t^I coherently in the amplitudes.

2.1. Results for $pp \to \pi^+ d$

There are data from Ref. [11] on the $pp \to \pi^+ d$ reaction and its time reversal reaction $\pi^+ d \to pp$, Ref. [19], in terms of $\pi^+ d \to pp$ cross sections. We convert these data into $pp \to \pi^+ d$ cross sections using the detailed balance theorem.

In Fig. 4 we show the results for $\sigma(pp \to \pi^+ d)$ as a function of $K_p^{\rm lab}$, the proton kinetic energy in the pp lab frame, the variable used in the data of Ref. [11], which are obtained

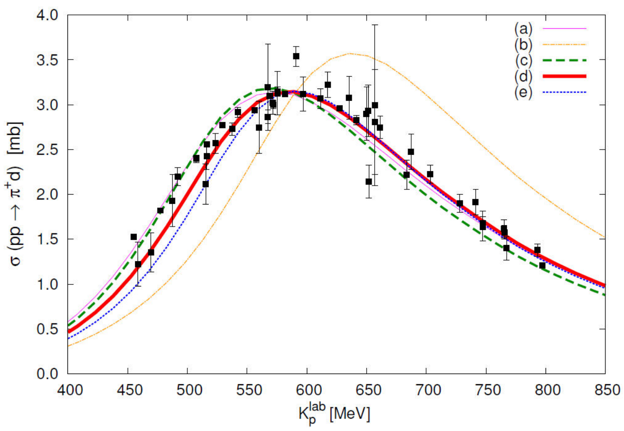

FIGURE 4. Cross section of $pp \rightarrow \pi^+ d$ as a function of the kinetic energy in the lab frame of the proton. The variable s is $s = 4M_N^2 + 2M_N K_p^{\rm lab}$.

by integrating $d\sigma/d\cos\theta_\pi$ of Eq. (6) over the pion angle, with the sum of all contributions given by Eq. (8).

We perform different fits to the data that require a detailed discussion. The parameters M_Δ, Γ_Δ, Λ_π, Λ_ρ, are varied keeping the coupling constants fixed. Five different fits are done to the data called (a)-(e).

The first fit, fit (a), is done to all the data in the range of $K_p^{\rm lab} \in$ [450:800] MeV. It presents a reduced χ^2/dof of the order of 9, which indicates a bad fit. The χ^2/dof is large because there are many data with tiny errors and some data are incompatible with other ones. This fit indicates that the solution of the fit prefers a mass lower than the nominal one, $M_\Delta = 1232$ MeV, and a width much larger than the experimental one of $\Gamma_\Delta = 117$ MeV. We think that the reason is that in the lower energy region of the data there must be other mechanisms additional to those considered here. We are not concerned about that since our purpose is to explain the data at a reasonable level to show the dominance of the Δ excitation and how the triangle singularity is exhibited.

We also tried to obtain a reasonable fit to the data fixing the mass and width of the Δ to the nominal ones. This is done in fit (b). The results are absolutely unacceptable as one can see in Fig. 4, with a reduced χ^2/dof of the order of 330. As one can see in Fig. 4, the data is definitely demanding a smaller Δ mass, closer to the pole mass of the PDG [20], as if the triangle singularity selected this mass rather than the Breit Wigner mass.

In view of this, we conduct another fit to the data restricting the range to reasonable values of the Δ mass and width, $M_\Delta \in$ [1200:1250] and $\Gamma_\Delta \in$ [100:150], and this is fit (c), which does not differ much from fit (a) at low proton energies but reduces the cross section a bit above the Δ peak.

Having admitted that we should not push our model to be too accurate with the data at low proton energies, we make two new fits, restricting the range of the data to $K_p^{lab} \in$ [525:700] and [550:700] MeV, which select the data closer to the Δ peak, and the same range for M_Δ and Γ_Δ than for fit (c). These fits are called (d) and (e). As we can see, both fits give a similar mass of around 1215 MeV and the width of fit (d) is $\Gamma_\Delta = 150$ MeV while for fit (e) is $\Gamma_\Delta = 117$ MeV. The χ^2/dof values have improved considerably (~ 4 and 2 for (d) and (e) respectively) when removing points from the region where our model would require other contributions. While fit (e) to the restricted data is acceptable, when observed in Fig. 4 versus all data, it is showing a large discrepancy with some of the low energy data with small errors. If we look at fits (c), (d) and (e), they provide a band that we could consider as uncertainty of our model in a fit to the data. This band region includes most of the data. In order to continue with the results for other observables given by our model, we select the fit (d) which is in the middle of the band to evaluate the results. We studied the different contributions in Ref. [17] and obtained that the pion exchange is the dominant term and the inclusion of the ρ exchange reduces substantially the cross section, as already found in Ref. [10], although not in Ref. [9] where the ρ contribution is moderate. On the other hand the effect of short range correlations is negligible and so is the effect of the impulse approximation.

The different contributions of the spin transitions are shown in Fig. 5.

We observe that the shape of the cross section depends on the channel. The transitions from the initial state $\uparrow\uparrow$ peak at higher energy, particularly the $\uparrow\uparrow\rightarrow\uparrow\uparrow$. However, those coming from the inital $\uparrow\downarrow$ (or $\downarrow\uparrow$ which are the same) peak around $K_p^{\rm lab} \simeq 600$ MeV, which is where one finds the peak of the total cross section. It is worth mentioning that the $\uparrow\downarrow\rightarrow\uparrow\uparrow$ and $\uparrow\downarrow\rightarrow\downarrow\downarrow$ transitions give the same contribution, while the largest one comes from $\uparrow\downarrow\rightarrow (1/\sqrt{2})(\uparrow\downarrow + \downarrow\uparrow)$. Altogether, we can claim that most of the cross section comes from the initial pp state $\uparrow\downarrow$ (or $\downarrow\uparrow$). This might be an indication that the $S = 0$ contribution is dominant and indeed this is the case. We find that it is the initial state combination $(1/\sqrt{2})(\uparrow\downarrow - \downarrow\uparrow)$ the one that is responsible for the transitions in this case. Thus, our model produces dominance of $S = 0$ in the pp initial state. This implies, because of the antisymmetry of the protons, that the orbital angular momen-

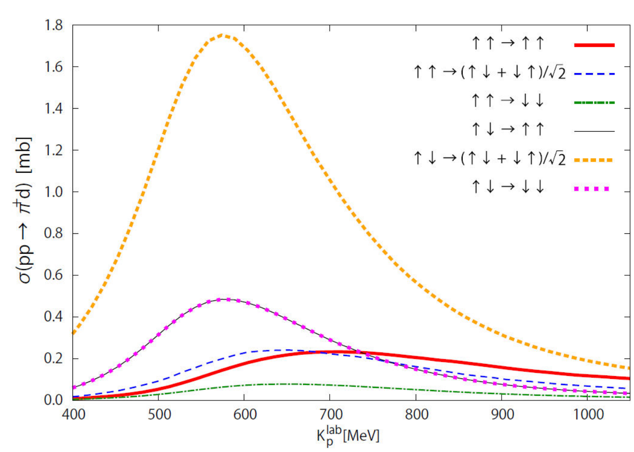

FIGURE 5. Contribution of the different spin transitions. A factor two is included to account for transitions from $\downarrow\uparrow$ and $\downarrow\downarrow$ which are identical to those of $\uparrow\downarrow$ and $\uparrow\uparrow$ respectively. Results obtained with set (d).

tum of the protons must be even. We could have $L=0, L=2$ in our model with pion exchange, however, since the correlation term, which selects the $L=0$ part, gives a negligible contribution, $S=0, L=2$ is the dominant contribution for the process. This initial state with $L=2$, $S=0$ ($^1D_2$) gives $J=2$, which means that the $\pi^+ d$ system also has $J=2$, and is in the $^3P_2$ configuration, ($^{2S+1}L_J$). It is interesting to note that this transition, $pp(^1D_2) \to \pi^+ d(^3P_2)$, is also the one that was found dominant in Ref. [21], and also in the experimental analysis of partially polarized data in Ref. [22], and more recently in Refs. [23,24]. It is also interesting to remark that, as in Refs. [23,24], the shape of the $^1D_2$ transition is very similar to the total cross section unlike for other partial waves. The angular distributions are also calculated [17] and they show a good agreement with data for kinetic energy of the proton $K_p^{\rm lab}$ of around 570 MeV. Here, we can extract some conclusions on the favored quantum numbers for the two-step mechanism of Fig. 1. To complete the total spin $J^{\rm tot}$ one needs now the angular momentum of the π^- produced in the $np(I=0) \to \pi^- pp$ step. One can see that $N^*(1440)N$ and the NN production in $np(I=0) \to \pi^- pp$ prior to the π^- emission play a relevant role, which makes the pion to couple in $L=1$ in this case. Then, it is easy to see that with $N^*(1440)$ or N excitation driven by pion exchange, the pions going forward for N^*-up (N-up) or backward for N^*-down (N-down), in the nomenclature given for the Δ excitation before, are preferred since this makes the pion propagator bigger. Hence, $L_z=0$ for this pion. The $|2,0\rangle$ state for $\pi^+ d$ and $|1,0\rangle$ for the π^- combine to $|J^{\rm tot},0\rangle$ with the Clebsch-Gordan coefficient $\mathcal{C}(2\,1\,J^{\rm tot};0\,0\,0)$. The Clebsch-Gordan coefficients squared give a factor $3/2$ from $J^{\rm tot}=3$ to $J^{\rm tot}=1$. Altogether, we arrive to the most favored production mode for the initial np system: $I=0$, $S=1$, $L=2$, $J^{\rm tot}=3$, the $^3D_3$ partial wave where a signal of the "$d^*(2380)$" is seen, and the configuration $I(J^P)=0(3^+)$ common to the initial and final state in the observed peak of the $np(I=0) \to \pi^+\pi^- d$ reaction [12].

3. The $np \to \pi^+\pi^- d$ cross section

The amplitude for the $np \to \pi^-\pi^+ d$ process in Fig. 1 is given by

$$-it'' = \frac{1}{2}\int \frac{d^4p_1}{(2\pi)^4}\frac{(2M_N)^2}{2E_N(p_1)2E_N(p_1')}\frac{i}{p_1^0-E_N(p_1)+i\epsilon} \times \frac{i}{\sqrt{s}-p_1^0-\omega_\pi-E_N(p_1')+i\epsilon}(-i)t\,(-i)t'. \quad (8)$$

The factor $1/2$ is to account for the intermediate propagator of two identical particles. In the d^4p_1 integrations t and t' would be off shell. Similarly to [4], the on-shell approximation allows one to write the cross section for $np \to \pi^+\pi^- d$ in terms of the $np(\mathrm{I}=0) \to \pi^- pp$ and $pp \to \pi^+ d$ ones. We use physical arguments to write the $np \to \pi^+\pi^- d$ cross section with an easy compact formula. We note that $\pi^0\pi^0$ or $\pi^+\pi^-$ in $I=0$ require an even value of their relative angular momentum l, and when $l=0$ the $\pi^0\pi^0$, or the symmetrized $(\pi^+\pi^- + \pi^-\pi^+)$, behave as identical particles, which reverts into a Bose enhancement when the two pions go together. Our argumentation is supported by the results of [1, 2] for $\pi^0\pi^0$ (see Fig. 2 of [1] and Fig. 4 of [2]). Then, we can write

$$\frac{d\sigma_{np\to\pi^+\pi^- d}}{dM_{\rm inv(\pi^+\pi^-)}} = \sigma_{np\to\pi^+\pi^- d}\,\delta(M_{\rm inv}(\pi^+\pi^-)-\bar{M}_{\pi\pi})\,. \quad (9)$$

We could take some $M_{\rm inv}(\pi^+\pi^-)$ distribution as input, but to make the results as model independent as possible we take the $\bar{M}_{\rm inv}(\pi^+\pi^-) \sim 2m_\pi + 60$ MeV, not far from threshold but we change it to see how the results depend on $\bar{M}_{\rm inv}$. The stability of the results that we find by changing the value of $\bar{M}_{\rm inv}(\pi\pi)$ justifies this approximation a posteriori. With this approximation we arrive to the final formula,

$$\sigma_{np\to\pi^+\pi^- d} = \frac{M_{\rm inv}(p_1p_1')}{6\pi}\frac{\sigma^I_{np\to NN\pi}\sigma_{pp\to\pi^+ d}}{M_{\rm inv}(\pi\pi)} \times \frac{\tilde{p}_1^2}{p_\pi p_\pi'}p_d\tilde{p}_\pi\,, \quad (10)$$

with $\sigma^I_{np\to NN\pi} = \sigma_{np(I=0)\to NN\pi}$ of [5,6]. In order to build a model independent solution we take the experimental data of the first and second step and we perform fits separately to both sets of data. We take data for $\sigma_{np(I=0)\to NN\pi}$ from Fig. 1 of [6]. Statistical and some systematic errors are considered in Ref. [5,6]. With the only purpose of making a realistic fit to the data we assume a typical 5% violation of isospin [25]. The systematic errors obtained are of the order of 0.5 mb in $\sigma_{np(I=0)\to NN\pi}$, which we also add in quadrature to the former ones of [6], and for the second step, $pp \to \pi^+ d$ we take the data of [11]. The $np(\mathrm{I}=0) \to NN\pi$ cross section is parameterized as $\sigma_i = \left|\alpha_i/(\sqrt{s}-\tilde{M}_i+i[\tilde{\Gamma}/2])\right|^2$, and call set I the one with the parameters: $\tilde{M}_1 = 2326$ MeV, $\tilde{\Gamma}_1 = 70$ MeV, $\alpha_1^2 = 2.6\left(\tilde{\Gamma}_1/2\right)^2$ mb MeV^2 ($\chi_r^2 = 0.50$), while set II has $\tilde{M}_2 = 2335$ MeV, $\tilde{\Gamma}_2 = 80$ MeV, $\alpha_2^2 = 2.5\left(\tilde{\Gamma}_2/2\right)^2$ mb MeV^2 ($\chi_r^2 = 0.52$). The $pp \to \pi^+ d$ cross section is parameterized as $\sigma_3 = \left|\alpha_3/(M_{\rm inv}(p_1p_1')-\tilde{M}_3+i[\tilde{\Gamma}_3/2])\right|^2$, with $\tilde{M}_3 = 2165$ MeV, $\tilde{\Gamma}_3 = 123.27$ MeV, $\alpha_3^2 = 3.186\left(\tilde{\Gamma}_3/2\right)^2$ mb MeV^2. In both cases we obtain good fits with $\chi^2/dof \simeq 1$. We show the results in Fig. 6.

In Table I we show the results obtained with set I and set II for the strength of $\sigma_{np\to\pi^+\pi^- d}$ at the peak, the peak position and the width of the peak, varying $\bar{M}_{\pi\pi}$, and $p_{1,\rm max}$ for the off shell calculations. What one sees is a stability of the results upon changes of $\bar{M}_{\pi\pi}$, which justifies the use of Eq. (9). We also find that off shell effects, justifying the on shell approximation used in Ref. [4]. The strength at the peak between $0.72-0.96$ mb should be considered quite good compared to the experimental one around 0.5 mb, given the different approximations done (fits to the $np(\mathrm{I}=0) \to \pi^- pp$ cross section with the systematic errors with $20-30\,\%$

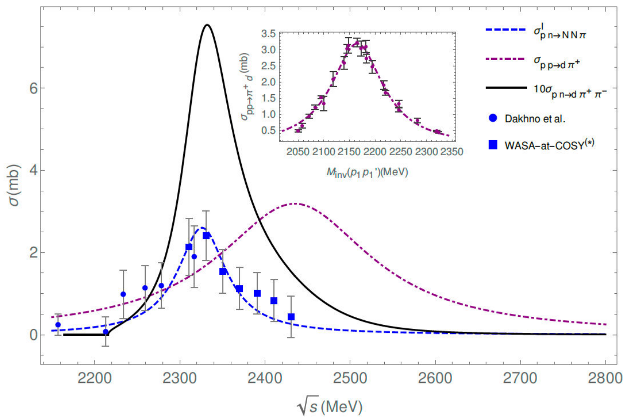

FIGURE 6. Plots of $\sigma_{np\to\pi^- pp}(I=0)$ and $\sigma_{pp\to\pi^+ d}$, as a function of $\sqrt{s}$ and $M_{\rm inv}(p_1 p_1')$, respectively. The results with $\sigma_{np\to\pi^+\pi^- d}$ in $I=0$ of Eq. (10) are multiplied by 10 for a better comparison. Results for set I and set II are similar [25]. Inset: $\sigma_{pp\to\pi^+ d}$ as a function of $M_{\rm inv}(p_1 p_1')$. Data for $pp\to\pi^+ d$ taken from [11]. Data for $np(\mathrm{I}=0)\to\pi NN$ are taken from Dakhno et al. [26], and WASA-at-COSY$^{(*)}$ [5, 6], including systematic errors from isospin violation.

smaller strength at the peak are still acceptable, hence such uncertainties in the resulting $np\to\pi^+\pi^- d$ cross section are expected). The peak position from $2332-2345$ MeV should also be considered rather good compared to the about 2365 MeV of the experiment [1–3, 5]. The narrow width observed in the experiment of $70-75$ MeV is also well reproduced by our results in the range of $75-88$ MeV.

The appeareance of the peak about 25 MeV below the experimental one is not significant with the perspective that, as discussed in Ref. [5], the authors achieve a resolution in $\sqrt{s}$ of about 20 MeV and the $pp\to pp\pi^0$ and $pn\to pp\pi^-$ cross sections, from where $\sigma_{np(\mathrm{I=0})\to pp\pi^-}$ is obtained via Eq. (14) of [25] with large cancellations, are measured using data bins of 50 MeV in T_p.

The derivation done contains the basic dynamical ingredients in a skilled way, making some approximations to rely upon experimental cross sections. We think that it is remarkable that a narrow peak, at about the right position, with strength and width comparable to the experimental peak of $np\to\pi^+\pi^- d$, appears in spite of the approximations done, and the stability of the results allows us to conclude that a peak with the properties of the experimental one associated so far to the “$d^*(2380)$” dibaryon is unavoidable from the mechanism that we have studied.

TABLE I. Values of the peak strength (“strength”), peak position (“position”), and width, for intermediate particles on shell (columns with $\delta\bar{M}_{\pi\pi}$, $\bar{M}_{\pi\pi}=2m_\pi+\delta\bar{M}_{\pi\pi}$), and off-shell (“o.s.”), where we have taken $p_{1,\rm max}=700$ and 800 MeV and $\delta\bar{M}_{\pi\pi}=60$ MeV.

	$\delta\bar{M}_{\pi\pi}$ (MeV)			$p^{\rm o.s.}_{1,\rm max}$ (MeV)	
Set I	40	60	80	700	800
strength (mb)	0.72	0.76	0.75	0.82	0.95
position (MeV)	2332	2332	2332	2332	2332
width (MeV)	76	76	81	75	75
Set II					
strength (mb)	0.75	0.80	0.80	0.85	0.96
position (MeV)	2342	2345	2345	2343	2342
width (MeV)	86	87	88	87	84

1. M. Bashkanov *et al.* Double-Pionic Fusion of Nuclear Systems and the ABC Effect: Aproaching a Puzzle by Exclusive and Kinematically Complete Measurements, *Phys. Rev. Lett.* **102** (2009) 052301.
2. P. Adlarson *et al.* [WASA-at-COSY], ABC Effect in Basic Double-Pionic Fusion — Observation of a new resonance?, *Phys. Rev. Lett.* **106** (2011) 242302.
3. P. Adlarson *et al.* [WASA-at-COSY], Isospin Decomposition of the Basic Double-Pionic Fusion in the Region of the ABC Effect, *Phys. Lett. B* **721** (2013) 229.
4. I. Bar-Nir *et al.* Analysis of the reaction n p → d pi+ pi- below 3.5 gev/c, *Nucl. Phys. B* **54** (1973) 17.
5. P. Adlarson *et al.* [WASA-at-COSY], Isoscalar single-pion production in the region of Roper and $d^*(2380)$ resonances, *Phys. Lett. B* **774** (2017) 599, [erratum: *Phys. Lett. B* **806** (2020 135555)]. `https://doi.org/10.1016/j.physletb.2017.10.015`.
6. H. Clement and T. Skorodko, On the Possibility of Dibaryon Formation near the N*(1440)N threshold, [arXiv:2010.09217 [nucl-ex]].
7. L. Alvarez-Ruso, E. Oset and E. Hernandez, Theoretical study of the N N —> N N pi pi reaction, *Nucl. Phys. A* **633** (1998) 519. `https://doi.org/10.1016/S0375-9474(98)00126-2`.
8. D. O. Riska, M. Brack and W. Weise, Pionic Disintegration of the Deuteron, *Phys. Lett. B* **61** (1976) 41.
9. A. M. Green and J. A. Niskanen, P Wave Meson Production in p p → d pi+, *Nucl. Phys. A* **271** (1976) 503.
10. M. Brack, D. O. Riska and W. Weise, Pionic Disintegration of the Deuteron, *Nucl. Phys. A* **287** (1977) 425.
11. C. Richard-Serre, W. Hirt, D. F. Measday, E. G. Michaelis, M. J. M. Saltmarsh and P. Skarek, A study of the reaction pi+ d → p p for pion energies between 142 and 262 mev, *Nucl. Phys. B* **20** (1970 413).

12. H. Clement and T. Skorodko, Dibaryons: Molecular versus Compact Hexaquarks, *Chin. Phys. C* **45** (2021) 022001. https://doi.org/10.1088/1674-1137/abcd8e.
13. M. Bayar, F. Aceti, F. K. Guo and E. Oset, A Discussion on Triangle Singularities in the $\Lambda_b \to J/\psi K^- p$ Reaction, *Phys. Rev. D* **94** (2016) 074039.
14. R. Karplus, C. M. Sommerfield and E. H. Wichmann, Spectral Representations in Perturbation Theory. 1. Vertex Function, *Phys. Rev.* **111** (1958) 1187.
15. L. D. Landau, On analytic properties of vertex parts in quantum field theory, *Nucl. Phys.* **13** (1960) 181. https://doi.org/10.1016/B978-0-08-010586-4.50103-6.
16. S. Coleman and R. E. Norton, Singularities in the physical region, *Nuovo Cim.* **38** (1965) 438,
17. N. Ikeno, R. Molina and E. Oset, Triangle singularity mechanism for the pp → π+d fusion reaction, *Phys. Rev. C* **104** (2021) 014614, https://doi.org/10.1103/PhysRevC.104.014614.
18. R. Machleidt, The High precision, charge dependent Bonn nucleon-nucleon potential (CD-Bonn), *Phys. Rev. C* **63** (2001) 024001.
19. SAID data base website: http://gwdac.phys.gwu.edu/b.
20. P.A. Zyla *et al.* [Particle Data Group], Review of Particle Physics, *PTEP* **2020** (2020) 083C01.
21. D. Schiff and J. Tran Thanh Van, A covariant theory of the pionic disintegration of the deuteron, Nucl. Phys. B **5** (1968) 529. https://doi.org/10.1016/0550-3213(68)90236-8.
22. M. G. Albrow et al., The reaction p p → pi+ d between 1.0 and 1.5 gev/c, *Phys. Lett.* **34B** (1971) 337.
23. R. A. Arndt, I. I. Strakovsky, R. L. Workman and D. V. Bugg, Analysis of the reaction pi+ d → p p to 500-MeV, *Phys. Rev. C* **48** (1993) 1926, [*Phys. Rev. C* **49** (1994 1229)]. https://doi.org/10.1103/PhysRevC.48.1926,10.1103/PhysRevC.49.1229.
24. C. H. Oh, R. A. Arndt, I. I. Strakovsky and R. L. Workman, Combined analysis of the reactions p p → p p, pi d →pi d, and pi d → p p, *Phys. Rev. C* **56** (1997) 635. https://doi.org/10.1103/PhysRevC.56.635.
25. R. Molina, N. Ikeno and E. Oset, Sequential single pion production explaning the dibaryon "$d^*(2380)$" peak, [arXiv:2102.05575 [nucl-th]].
26. L. G. Dakhno *et al.* MEASUREMENT OF THE CROSS-SECTION OF THE REACTION P N → P P PI- IN THE ENERGY REGION OF DIBARYON RESONANCES (500-MEV - 1000-MEV), *Phys. Lett. B* **114**, 409-413 (1982) https://doi.org/10.1016/0370-2693(82)90081-8.